

An interface element to model the mechanical response of crease lines for carton-based packaging

Umberto Perego¹, Andrea Giampieri¹

¹*Department of Structural Engineering, Politecnico di Milano, Italy*

E-mail: umberto.perego@polimi.it, giampieri@stru.polimi.it

Keywords: Crease lines, interface elements, inelastic traction/displacement constitutive laws.

SUMMARY. Paperboard is one of the most widely used materials in industrial processes, notably for packaging purposes. Packages are obtained through a continuous forming process, in which a flat laminated sheet is converted into the final 3-D solid. In the package forming process, it is common practice to score the paperboard laminate with crease lines, in order to obtain folds with sharp edges and to minimize the initiation and propagation of flaws during the subsequent folding procedures. In this work, a constitutive model for the mechanical response of crease lines is proposed and validated on the basis of experimental tests available in the literature.

1 INTRODUCTION

Paperboard is a composite laminate material, made of a stack of paper plies obtained from the manufacturing of different pulps of vegetable fibers; the multilayered structure is employed in order to increase the bending stiffness of the laminate, as commonly done in sandwich plates (fig. 1(a)). In the industrial lamination process, fibers tend to align along the so-called *Machine Direction*, thus paperboard is usually modeled as an orthotropic medium.

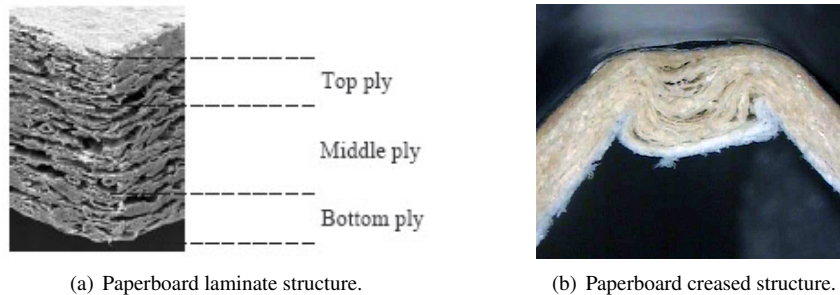


Figure 1: Paperboard structure.

In the forming process of packages containing beverages, a flat laminated sheet of paperboard is converted into a cylinder, it is longitudinally sealed, it is filled with liquid and then transformed into the final 3-D solid. At the end of this process, the cylindrical paperboard is folded and it is given its final box-like shape. The formation of folds along narrow lines is facilitated by pre-scoring the paperboard with so-called crease lines. The creasing technology takes advantage of the stratified structure of the paperboard, by promoting inter- and intra-ply delaminations (fig. 1(b)), to locally reduce the bending stiffness and strength of the material along a predetermined pattern of lines (fig. 2(a)), in correspondence of the edges of the package.

2 THE CREASING PROCESS

A couple of male and female dies (fig. 2(b)) is used to indent the paperboard along a straight line, in order to locally weaken the fiber structure. The main mechanisms responsible for the damaging of the paperboard structure under creasing are: (1) the development of in-plane inelastic deformations; (2) the development of delamination defects, caused mainly by out-of-plane shearing strains; these flaws are positioned inside the board in correspondence of the sidelong gaps between the male die and the female channel; (3) the partial opening of the cracks between layers during unloading, caused mainly by through-the-thickness stresses normal to the ply interfaces, where the cohesive forces are activated, which results in a residual bulge of the creased region at male die unloading.

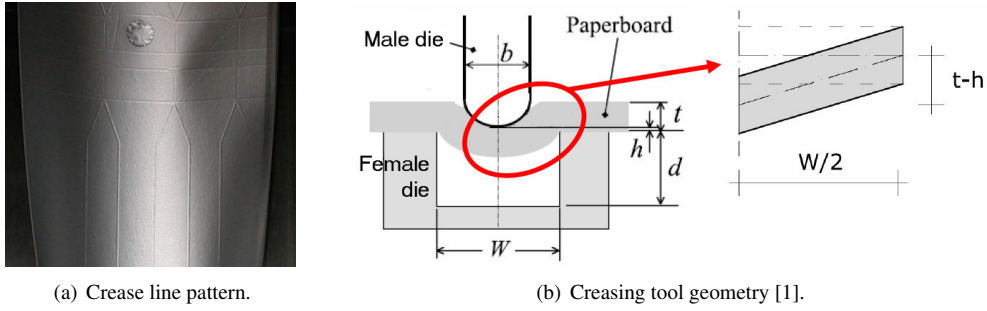


Figure 2: Creasing procedure.

Experimental evidences show that, when paperboard is bent without being creased, cracks appear on the outer surface; thus the correct design of the creasing tool is fundamental to guarantee good lifetime performances of the package, since the resulting mechanical properties of the crease lines depend on the creasing tool geometry: (1) the diameter and the shape of the male die; (2) the channel width; (3) the indentation depth. The effect of these three factors is usually summarized in the industrial community by the so-called RCS (Relative Crease Strength), which is defined as the ratio between the bending force registered during a standard folding test (fig. 3), performed over the creased material, and the bending force which is needed to fold the uncreased material.

Nagasawa et al. [1] performed experimental studies on both creasing and folding; they tested different kinds of paperboard, varying creasing tool parameters in order to investigate the crease line response. Since the out-of-plane shearing strain can be considered one of the main causes for the development of delamination defects, Nagasawa et al. [1] defined a non-dimensional *nominal initial shearing strain* parameter to characterize the creasing process (fig. 2(b)), in the form:

$$\gamma = \frac{2(t-h)}{W} \quad (1)$$

where t is the paperboard thickness, h is the final position of the male die at maximum indentation depth and W is the channel half-width. According to this definition, γ represents the ratio between the creasing penetration and the channel half-width, thus defining an overall measure of the imposed shearing strain.

The experimental bending moment vs. rotation angle curves obtained by Nagasawa et al. by submitting paperboard specimens, creased at different values of γ , to standard bending tests about the crease axis (fig. 3), are shown in figure 4(a). A transition value, separating deep creasing from shallow creasing, can be identified at $\gamma_{tr} = 0.6$. A summary of the mechanical properties of the

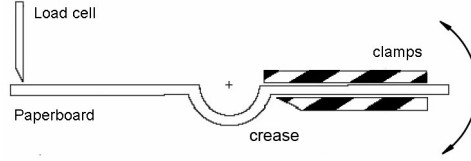


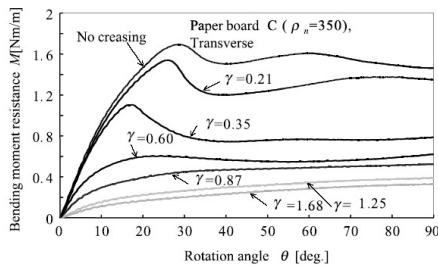
Figure 3: Schematic view of the typical bending force tester.

cross-direction-creased paperboard tested by Nagasawa et al. [1] is given in table 1, where $\sigma_{B,MD}$ is the nominal tensile strength of paperboard in machine direction, while $\varepsilon_{B,MD}$ is the ultimate strain in the same direction.

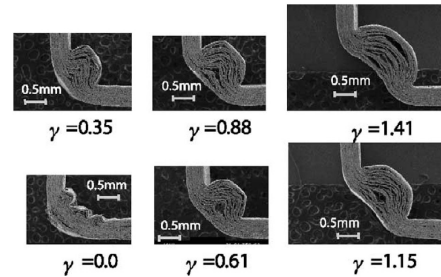
Table 1: Mechanical properties of the sample paperboard, in the Machine Direction, taken from [1] (product C).

thickness $t(\text{mm})$	nominal tensile strength $\sigma_{B,MD}(\text{MPa})$	nominal strain $\varepsilon_{B,MD}(\%)$
0.46	46	5.1

For shallow-indentated crease lines, a softening post-peak branch is observed, while for deep-indentated creases, perfect plasticity is the dominant dissipative mechanism.



(a) Bending curves, for different values of γ .



(b) Sectional views of bent crease lines, for different values of γ .

Figure 4: Bending test results, reported by Nagasawa et al. [1].

As noticed by several Authors (see, e.g., [2] and [3]), the paperboard failure in compression is characterized by delamination due to buckling of the compressed layers. In increased or shallow-creased specimens this leads to an abrupt release of elastic energy with a sharp reduction of bending strength, which accounts for the peak followed by a softening branch in the bending curves of this type of creased specimens (fig. 4(a)), for low values of γ ($\gamma < 0.6$). In the presence of deep creasing ($\gamma > 0.6$), the local bending stiffness is reduced by the delamination produced by the creasing process so that the energy release, due to the progression of damage during bending, is gradual and it does not produce any visible peak in the bending curves (fig. 4(a)). This behaviour is evidenced by the pictures in figure 4(b), showing 90° folds of paperboard specimens, characterized by increasing values of γ .

For small values of γ , little delamination is visible, while the layers on the tensile side appear to be deteriorated: the elastic response is stiffer and much elastic energy is stored during elastic loading; the peak corresponds to the sudden propagation of delamination, as the elastic energy is partially released by the triggering of unstable fracture propagations, due to the buckling of the outer layers.

For larger values of γ , the preliminary creasing procedure generates a large number of delamination defects, which evolve into layer detachments during folding. The buckled layers produce a well defined bulge on the compressed side, giving rise to a neat folding line with sharp edges. In this case no softening branch is observed, as delamination evolves in a stable manner. A plateau is reached in the bending curve, where rotations about the crease line may occur without any increase in the moment resistance, as the buckling-induced deflections evolve under constant compressive loads; in these cases the crease line behaves like a cylindrical plastic hinge.

3 CREASE INTERFACE ELEMENT

Paperboard is conveniently modeled by shell elements, standing the small thickness of the laminate if compared to the other sheet dimensions. In view of its small width, it is also convenient to discretize the crease line by interface elements, interposed between two adjoining shell elements (fig. 5(a)). A zero-thickness 2-noded linear interface element (fig. 5(b)) is proposed to model the presence of crease lines; it is intended to be used between 4-noded, Mindlin-Reissner shell elements, of the MITC4 type [4]. The shell element configuration is described by the definition of its midsurface

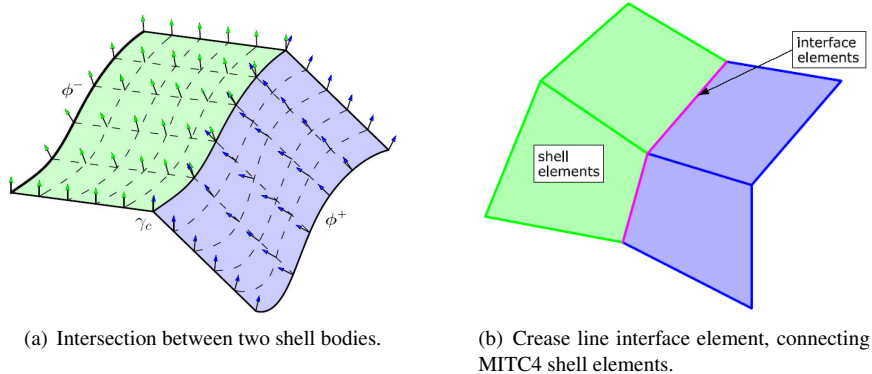


Figure 5: Shell and interface elements.

plus a director vector field; the shell element is thus characterized by 5 degrees of freedom per node (three displacements and two incremental rotations).

The 3D displacement field in the creased region is modeled in the zero-thickness interface element by interpolating the midsurface displacement jump and the director rotation jump between facing nodes of the shell elements connected to the interface.

The *crease surface*, connecting two shell bodies, is shown in figure 6(a); it can be used to define a local, orthonormal, co-rotational reference frame $\{\hat{\mathbf{V}}_n, \hat{\mathbf{V}}_c, \hat{\mathbf{V}}_t\}$ along the crease line (fig. 6(b)), where $\hat{\mathbf{V}}_c$ is aligned with the tangent to the midsurface crease axis, $\hat{\mathbf{V}}_n$ is normal to the crease surface and $\hat{\mathbf{V}}_t = \hat{\mathbf{V}}_n \times \hat{\mathbf{V}}_c$. As creasing is intended to weaken the bending properties of the laminate along the folding line, only rotations about the interface element axis $\hat{\mathbf{V}}_c$ are expected to

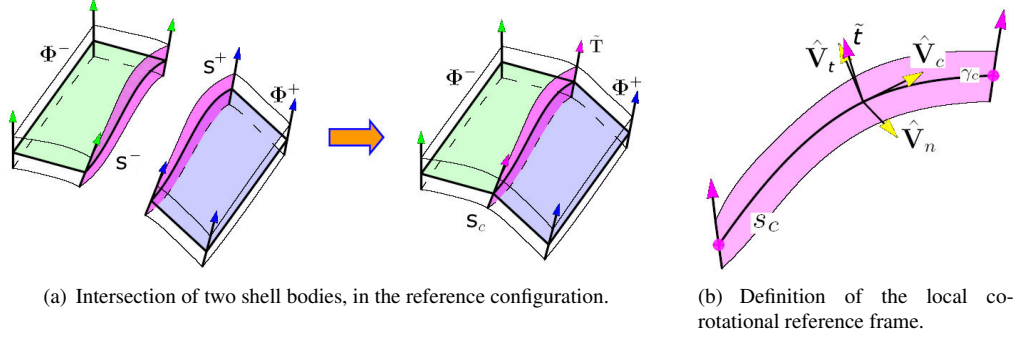


Figure 6: Crease surface.

be large; this relative rotation component has been considered to be the dominant factor affecting the crease nonlinear mechanical response. Large rotation jumps are treated as sequences of small rotations about mobile axes updated at every time increment, that is by exploiting the hypothesis of small rotation increments in the time-advancing step, which is a reasonable assumption in view of the explicit strategy adopted for the time integration of the discrete equations of motion.

The generalized stress ($\hat{\boldsymbol{\sigma}}$) and strain ($\hat{\boldsymbol{\epsilon}}$) vectors for the interface element can be written with reference to the local co-rotational basis, aligned with the crease axis:

$$\hat{\boldsymbol{\sigma}} = \{\hat{m} \ \hat{n} \ \hat{q}_c \ \hat{q}_t\}^T \quad \hat{\boldsymbol{\epsilon}} = \{\hat{\theta} \ \hat{w}_n \ \hat{w}_c \ \hat{w}_t\}^T \quad (2)$$

where \hat{m} is the bending moment about the crease axis, \hat{n} is the generalized axial force normal to the crease surface, while $\hat{\mathbf{q}}$ is the vector of the generalized shear forces; their conjugate quantities are: $\hat{\theta}$, the total rotation about the crease axis, and $\hat{\mathbf{w}}$, which is the displacement jump vector between the adjoining midsurfaces.

4 MULTI-SCALE APPROACH

Starting from the meso-scale model proposed by Carlsson et al. [5], a parallel-beam approach is adopted to interpret the crease interface constitutive behaviour. The crease-equivalent section is treated like a set of beams in parallel (fig. 7(b)), a hypothesis which is in agreement with the mechanisms activated in the damaged region during the creasing procedure (fig. 7(a)). The assumption is made that creasing generates a subdivision of the paperboard section in N layers, clamped at their ends, which are going to separate under folding; a simple *free mode* type of buckling is assumed for each layer, neglecting their mutual contact and interaction. The purpose of this model is the investigation of the variation of the crease response as a consequence of an increase in the severity of the preliminary creasing procedure. For higher values of γ , more delamination defects are generated, thus: (1) the extension L of the damaged region (parallel-beam length) increases (fig. 7(b)); (2) the number N of layers increases (resulting in a reduction of the parallel-beam height); (3) the residual bulge after creasing is more prominent (the initial deflection of the parallel-beam increases); thus, an increase in both the slenderness and the initial imperfection of each parallel-beam occurs.

In figure 8, a scheme of the multi-scale approach is shown. At the meso-scale level, paper is idealized as a simplified elastic - perfectly plastic material, with symmetric behaviour between tension and compression. At the macro-scale, paperboard is assumed to have a homogeneous compact section, characterized by a perfectly plastic, non-symmetric between tension and compression, in-plane

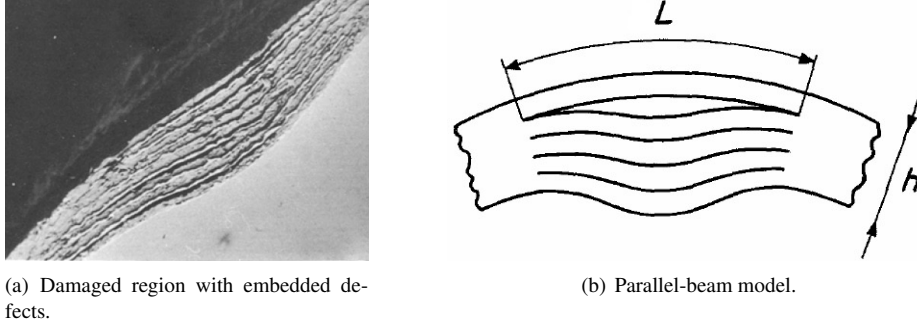


Figure 7: Damaged region after creasing ([3],[5]).

behaviour. Since the failure in compression is due to the occurrence of local buckling phenomena, the macroscopic behaviour in compression is desumed from the stability curves obtained from the meso-scale model, describing the load-bearing capacity of the parallel-beams. For increasing values of γ , the yield limit in compression of the macro-scale paperboard material is scaled with a law obtained by fitting the stability curves, in the form:

$$\hat{n}_y^c(\gamma) = \left(\frac{\hat{n}_y^{c0} - \hat{n}_y^{c1}}{2} \right) \tanh[-\nu_{nc} f_{nc}(\gamma) + \omega_{nc}] + \left(\frac{\hat{n}_y^{c0} + \hat{n}_y^{c1}}{2} \right) \quad (3)$$

where \hat{n}_y^{c0} and \hat{n}_y^{c1} are the yield limits for the limit values (γ^0, γ^1) of the range of interest of γ , while ν_{nc} and ω_{nc} are two parameters representing respectively the slope of the hyperbolic function at its center and a translation of the center of the curve; they need to be calibrated on the basis of experimental tests; $f_{nc}(\gamma)$ is a transformation function to pass from the range of interest of the nominal shearing strain $\gamma \in (\gamma^0, \gamma^1)$ to the range of the hyperbolic function $(-\infty, +\infty)$, in the form:

$$f_{nc}(\gamma) = - \left(\frac{\gamma_{nc}^c - \gamma^0}{\gamma - \gamma^0} \right)^2 + \sqrt{\frac{\gamma_{nc}^c - \gamma^1}{\gamma - \gamma^1}} \quad (4)$$

where γ_{nc}^c defines a center for the hyperbolic function. On the contrary, the value of the yield limit in tension is held constant with γ , namely $\hat{n}_y^t(\gamma) = \hat{n}_y^{t0}$.

5 INTERFACE CONSTITUTIVE MODEL

Paperboard can be considered as an elastic medium, with inelastic dissipation intentionally localized in the crease lines and incorporated in the interface constitutive law, expressed in terms of stress resultants *vs.* displacement and rotation jumps, as customary in interface formulations.

As discussed in section 2, when folding tests are performed on shallow-indented crease lines, a softening post-peak branch is observed in the bending response, while for deep-indented crease lines, perfect - plasticity can be regarded as the dominant dissipative mechanism.

The proposed interface model is defined in terms of generalized stress and strain components, expressed in the co-rotational reference frame. The additive decomposition of the strain components is assumed, in the form:

$$\hat{\epsilon} = \hat{\epsilon}^e + \hat{\epsilon}^p \quad (5)$$

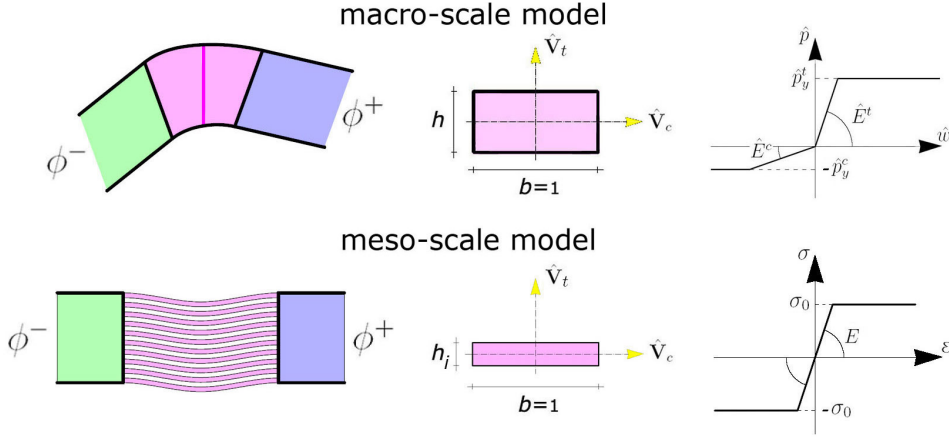


Figure 8: Summary of the two scales employed for the description of the creased region.

An ad hoc elastic - perfectly plastic constitutive model with damage, based on the hypothesis of strain equivalence [6], is proposed for the modeling of the mechanical response of the creased region. The elastic relations can be written in the form:

$$\hat{\sigma} = \hat{\mathbf{E}}^\diamond \hat{\epsilon}, \quad \hat{\sigma}^\diamond = \hat{\mathbf{E}} \hat{\epsilon} \quad (6)$$

where the superscript $\hat{\sigma}^\diamond$ denotes the effective stress vector, while $\hat{\mathbf{E}}^\diamond$ is the elastic damaged tensor. A linear hyperelastic relation has been assumed, inside the elastic domain. The elastic response in the local reference frame is supposed to be uncoupled, that is the elastic tensor $\hat{\mathbf{E}}$ is represented by a diagonal matrix: $\hat{\mathbf{E}} = \text{diag}\{k_\theta, k_n, k_c, k_t\}$. The relation between the generalized shear components and their conjugate displacement jumps are assumed to be governed by a purely linear elastic response. The existence of a thermodynamic potential is postulated, from which the interface state laws can be derived. A generalized Helmholtz free energy function $\hat{\Psi}$ is defined in the form:

$$\hat{\Psi} = \frac{1}{2}k_c \hat{w}_c^2 + \frac{1}{2}k_t \hat{w}_t^2 + \frac{1}{2}k_n^c \langle \hat{w}_n^e \rangle_-^2 + \frac{1}{2}k_n^t \langle \hat{w}_n^e \rangle_+^2 + \frac{1}{2}(1 - d_\theta)k_\theta \hat{\theta}^2 \quad (7)$$

where d_θ is the damage variable introduced to affect the bending behaviour. An elastic domain in the space of effective bending moment vs. generalized axial force is defined, in agreement with the $M - N$ interaction domains employed in the limit analysis of plates. Associativity is assumed for the evolution laws of plastic deformations, within the framework of classic rate-independent plasticity. The $M - N$ interaction domain can be defined by evaluating the M-N limit domain for an equivalent section of constant height, which is assigned the macro-scale material model discussed in section 4. The yield surface, bounding the elastic domain, can be written in the form:

$$\hat{f}_i(\hat{n}, \hat{m}^\diamond) = A\hat{n}^2 + B\hat{n} + (-1)^{i+1}C\hat{m}^\diamond - 1 \quad i = 1, 2 \quad (8)$$

where the coefficients $\{A, B, C\}$ are functions of the yield limits in compression \hat{n}_y^c and in tension

\hat{n}_y^t , in the form:

$$A = \frac{1}{\hat{n}_y^c \hat{n}_y^t} \quad (9)$$

$$B = \frac{\hat{n}_y^c - \hat{n}_y^t}{\hat{n}_y^c \hat{n}_y^t} \quad (10)$$

$$C = \frac{2}{h} \left(\frac{\hat{n}_y^c + \hat{n}_y^t}{\hat{n}_y^c \hat{n}_y^t} \right) \quad (11)$$

Perfect plasticity is assumed; the associated flow rules, with the corresponding loading/unloading conditions, are then given in the form:

$$\dot{\epsilon}_d^p = \sum_{i=1}^2 \frac{\partial \hat{f}_i}{\partial \hat{\sigma}_d^\diamond} \dot{\lambda}_i, \quad \hat{f}_i(\hat{n}, \hat{m}^\diamond) \leq 0 \quad \dot{\lambda}_i \geq 0 \quad \hat{f}_i(\hat{n}, \hat{m}^\diamond) \dot{\lambda}_i = 0 \quad (12)$$

The damage variable d_θ is introduced (eq. 7) to model the degradation of the generalized bending stiffness under the progressive onset and propagation of delaminations inside the creased laminate structure. The bending stiffness degradation has been related to the reduction of the moment of inertia I_c of an equivalent section, due to the reduction in the effective height caused by the detachment of the buckled layers. If a sectional damage variable d_s is defined as the ratio between the buckled layers and the total number of layers composing the paperboard structure, then the generalized damage variable d_θ can be related to this sectional damage variable d_s , according to the following equations:

$$I_c^d \simeq (1 - d_s)^3 I_c^0, \quad k_\theta^\diamond = (1 - d_\theta) k_\theta, \quad d_\theta = d_s^3 - 3d_s^2 + 3d_s \quad (13)$$

Delamination is assumed to be promoted by the attainment of a critical shortening strain in the compressed layers, hence an equivalent shortening strain $\hat{\epsilon}_{eq}$ is assumed to govern the evolution of the sectional damage d_s . It is defined to be a function of the half-thickness of the section $h/2$, of the total elastic rotation jump $\hat{\theta}^e$, of a cumulated measure of plastic rotation jump \hat{v}^p and of a weighted measure of the average shortening of the creased region \hat{w}_n , in the form:

$$\hat{\epsilon}_{eq} = \frac{h}{2} \left(|\hat{\theta}^e| + \hat{v}^p \right) - c_{dw} \hat{w}_n \quad (14)$$

The state of damage is characterized by a damage activation criterion in the form:

$$g(\hat{\epsilon}_{eq}, \hat{\epsilon}_{eq}^s) = \hat{\epsilon}_{eq} - \hat{\epsilon}_{eq}^s \leq 0 \quad \forall t \in \mathbb{R}_+ \quad (15)$$

where $\hat{\epsilon}_{eq}^s$ represents the damage threshold at current time t . The evolution laws for the damage variable and the damage threshold, in the range $d_s \in [0, 1]$, can be written in terms of a non-negative damage multiplier $\dot{\mu}$; here a simple linear law is proposed, as a function of only two parameters (the damage limit d_s^{lm} and the corresponding equivalent strain limit $\hat{\epsilon}_{eq}^{lm}$), in the form:

$$\dot{d}_s = \frac{d_s^{lm}}{\hat{\epsilon}_{eq}^{lm}} \dot{\mu}, \quad \dot{\hat{\epsilon}}_{eq}^s = \dot{\mu} \quad (16)$$

together with the corresponding damage loading/unloading conditions:

$$\dot{\mu} \geq 0 \quad g(\hat{\epsilon}_{eq}, \hat{\epsilon}_{eq}^s) \leq 0 \quad \dot{\mu} g(\hat{\epsilon}_{eq}, \hat{\epsilon}_{eq}^s) = 0 \quad (17)$$

where the value of $\dot{\mu}$ can be determined, in the case of damage loading, by the enforcement of the damage consistency condition $g = \dot{g} = 0 \Rightarrow \dot{\mu} = \dot{\hat{\epsilon}}_{eq}$.

6 RESULTS

The proposed model has been calibrated on the bending tests (fig. 3) performed by Nagasawa et al. [1]. The interface constitutive model, introduced in section 5, for an assigned value of γ , needs the calibration of 10 parameters. By use of the concepts at the base of the multi-scale approach, exposed in section 4, a set of interpolation functions has been proposed to capture the variation of the interface constitutive parameters in the range of interest of $\gamma \in (0, 1.7)$. Six different creasing configurations have been tested: the uncreased case, two shallow-creased cases, the transition case and two deep-creased cases. The comparison between the experimental results and the bending curves obtained with the proposed interface model (fig. 9) shows that the proposed simplified model is able to capture the main features of the crease response in the whole range of interest of γ . As a

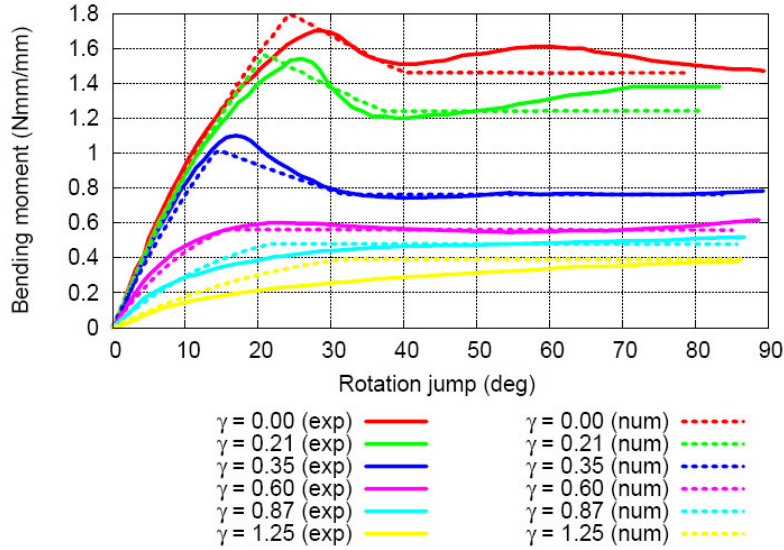


Figure 9: Comparisons between numerical results, obtained with the proposed crease model, and experimental results [1] for the crease bending curves, for increasing values of γ .

result of the calibration, the transition between the shallow-creased and the deep-creased cases, that is the transition from the peak-and-softening behaviour to the plastic-hinge-like behaviour of the creased region, is well captured by the crease model. Figure 10(a) shows the reduction of the compressive yield limit of the macro-scale material due to the reduction of the load-bearing capacity of the parallel-beams under buckling-plasticity interaction. The M-N interaction domain is symmetric only in the uncreased case ($\gamma = 0$). In figure 10(b) the numerical and the experimental trends of the maximum bending moment resistance are compared; the crease model shows good agreement with the experimental results.

7 CONCLUSIONS

An interface element and its corresponding crease constitutive model have been formulated for the modeling of the folding behaviour of creased paperboard. The use of the simplified parallel-beam approach provides a mechanical foundation for the interpretation of the dependence of the folding behaviour on the initial shearing parameter γ and it allows, through the use of simple interpolations,

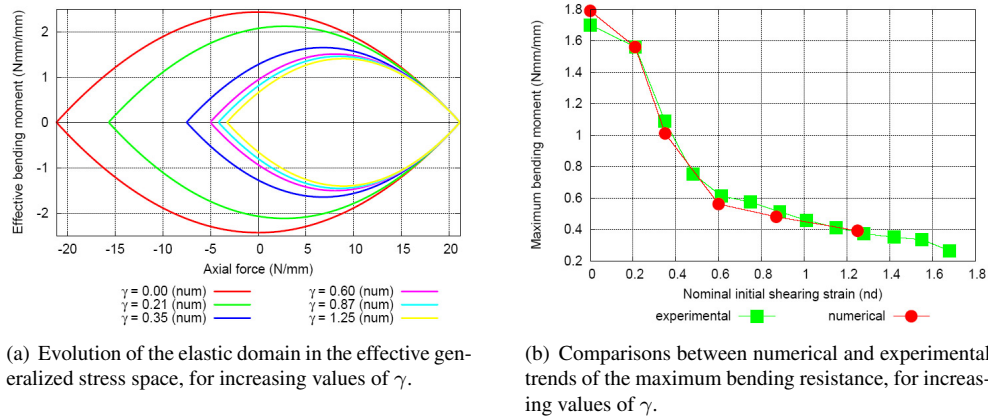


Figure 10: Comparisons between numerical and experimental [1] results.

to obtain quantitative predictions on the resulting material properties.

Numerical results obtained with the proposed crease model show good agreement in comparison to experimental results published in the literature [1], when the simulation of the standard bending test is performed.

The proposed interface elements are intended to be used for the simulation of the packaging forming process and as a numerical tool for the optimization of the crease pattern design.

References

- [1] Nagasawa S. and Fukuzawa, Y. and Yamaguchi, T. and Tsukatani, S. and Katayama, I., "Effect of crease depth and crease deviation on folding deformation characteristics of coated paperboard." *Journal of Materials Processing Technology*, **140**, 157-162 (2003).
- [2] Cavlin, S. and Dunder, I. and Edholm, B., "Creasability testing by inclined rules - a base for standardized specification of paperboard." *Packaging Technology and Science*, **10**, 191-207 (1997)
- [3] Carlsson, L. and Fellers, C. and Ruvo, A., "The mechanism of failure in bending of paperboard." *Journal of Materials Science*, **15**, 2636-2642 (1980)
- [4] Bathe, K.J. and Chapelle, D., *The Finite Element Analysis of Shells: Fundamentals*, Springer Verlag, Wien (2003).
- [5] Carlsson, L. and De Ruvo, A. and Fellers, C., "Bending properties of creased zones of paperboard related to interlaminar defects." *Journal of Materials Science*, **18**, 1365-1373 (1983)
- [6] Lemaitre, J. and Chaboche, J.L., *Mechanics of Solid Materials*, Cambridge University Press, (1990).